Evolution of Disorder in Two-Dimensional Stripe Patterns: "Smectic" Instabilities and Disclination Unbinding

M. Seul and R. Wolfe
AT&T Bell Laboratories, Murray Hill, New Jersey 07974
(Received 22 August 1991)

A combination of video polarization microscopy and extensive digital line pattern analysis has been invoked to examine in quantitative detail the transformation of a lamellar into a "labyrinthine" magnetic-stripe domain pattern. The evolution of disorder is found to be mediated by a sequence of transverse, "smectic" instabilities culminating in the generation of disclination dipoles. Their subsequent continuous "unbinding" facilitates the formation of a globally isotropic nonequilibrium pattern adopting the topology of a binary tree and displaying a well-defined morphology with a motif in the form of oblong, polygonal clusters of linear-stripe segments.

PACS numbers: 61.70.−r, 05.70.Fh, 64.70.−p, 75.70.Kw

Uniaxially modulated states abound in both two- and three-dimensional condensed-matter systems. Widely studied examples include the following: the ubiquitous lamellar or smectic phases of liquid crystals [1], surfactants [2], and block copolymers [3]; linear arrays of domain walls or discommensurations stabilized by competing periodicities such as those of rare-gas atomic and simple molecular adsorbate layers and the crystalline substrates on which they are deposited [4], as well as those of intercalates and their graphite host [5]; steps decorating reconstructed surfaces of certain semiconductors [6] and metals [7]; and stripe domain phases in ferrofluids [8], Langmuir monolayers [9], and thin magnetic garnet films [10], favored by the competition between a local attractive interaction, manifesting itself in the form of a domain-wall energy, and a repulsive electrostatic or magnetostatic interaction of long range [11]. The latter class of materials, long the subject of a substantial and ongoing effort to realize a variety of devices [12], has recently received renewed attention focusing on dynamic as well as structural aspects of their characteristic "stripe" and "bubble" phases [11]. Topological considerations play an essential role, whether they pertain to the cellular network of coarsening bubble domains [13], to the melting of bubble lattices [14], to the sequence of domain-wall bifurcations in thick garnet films [15], or to the constraints governing a complex variety of disordered, nonequilibrium stripe patterns [16].

In this Letter we investigate the evolution of disorder in the two-dimensional lamellar ground state of magnetic-stripe domains transforming the initial ordered pattern into a globally isotropic "labyrinthine" pattern [16–18]. We show that this process is mediated by a sequence of transverse instabilities bearing a close resemblance to those of smectic liquid crystals subjected to compressive or dilative stress [19], and culminating in the formation and subsequent "unbinding" of disclination dipoles. The emerging nonequilibrium labyrinthine patterns exhibit a characteristic density of disclination defects, symmetrically distributed between the two components of magnetization and imparting on each the topology of a binary tree. This network of disclinations delineates a well-defined local structure whose motif is an oblong cluster of parallel line segments of characteristic size and shape, analyzed in detail elsewhere [18,20].

Experiments were performed on ferrimagnetic garnet films of composition $(YGdTm)_3(FeGa)_5O_{12}$, grown epitaxially on the (111) face of gadolinium gallium garnet substrates to a thickness of approximately 13 μm. These films are characterized by a saturating magnetic field of approximately 70 Oe at room temperature, a uniaxial anisotropy of greater than 30:1, and a (zero-field) critical temperature of approximately 192 °C. Domains of alternating "up" and "down" magnetization were visualized in a transmission polarization microscope aligned for Köhler illumination, relying on the Faraday effect and the contrast enhancement afforded by video detection [21]. Digital image analysis was performed on a system described previously [22], employing a set of algorithms for line pattern analysis of which a detailed exposition is given elsewhere [20].

To generate the lamellar patterns exemplified by Fig. 1(a), films were cooled from the paramagnetic phase in the presence of a small ($H_\parallel < \frac{1}{2}$ Oe) symmetry-breaking intraplanar, but zero normal ($H_\perp = 0$ Oe) field [16,18,23]. The temperature dependence of the lamellar spacing, $d = d_{H_\perp = 0}(T) = 2\pi/q$, analyzed elsewhere [23,24], requires adjustment of the number $N = L_0/d$ of stripes present in a lamellar pattern of area $A \simeq L_0^2$. During cooling, this adjustment, implying the "coarsening" of the pattern, is facilitated by the generation and glide of dislocation pairs; this mediates the expulsion of affected stripes, a phenomenon analogous to what has been recently reported in the context of convective roll patterns [25]. In contrast, the increase in the density of stripes implied by heating requires the "injection" of additional stripes if the lamellar state is to be maintained. This is not observed. Instead, heating of the lamellar phase, realized at a temperature T_0, induces a transverse instability of the ordered stripe pattern, as illustrated in Fig. 1, and mediates the eventual formation of a globally disordered, labyrinthine state via the formation and unbinding of disclination dipoles.

Optical diffraction spectra demonstrate that the lamellar ground state first becomes unstable to a single transverse mode, corresponding to a sinusoidal modulation.

Inspection of transient intermediate states yielding the fully evolved undulation (or "buckling") instability depicted in Fig. 1(b) reveals the amplitude growth to be continuous. From the diffraction pattern [26], the wavelength, $\lambda_\perp \equiv 2\pi/q_\perp$, of the unstable mode is found to be $\lambda_\perp \simeq 10 d_0$, where $d_0 \equiv d(T_0)$ denotes the fundamental modulation period at onset. Further compression transforms the undulation pattern of Fig. 1(b) continuously into a chevron (or "zigzag") pattern, illustrated by Fig. 1(c) and characterized by a Fourier spectrum containing a set of "off-axis" peaks ($q_\perp \neq 0$). Intermediate spectra document the gradual appearance of higher harmonics of the transverse modulation and the concomitant disappearance of intensity in the longitudinal ($q_\perp = 0$) harmonics of the original lamellar pattern. A characteristic set of diffraction spectra is shown elsewhere [26].

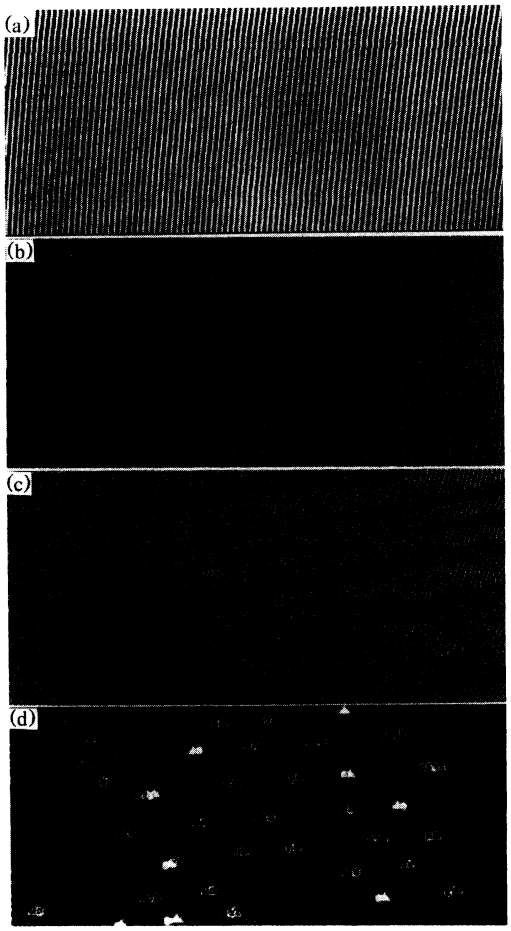

FIG. 1. (a) Transverse instability of lamellar pattern and the resulting (b) undulation and (c) chevron patterns, driven by temperature-induced dilative strain in zero field. (d) The formation of disclination dipoles in both components of the pattern ["black" (▲,●) and "white" (△,○); see also Fig. 2] generates a two-dimensional structure containing characteristic rhombohedral plaquettes. In (b)–(d), only the medial axis transform ("skeleton") [18,20] of the original "white" pattern component is shown. The stripe period, $d_0 \equiv d(T_0)$, in (a) is 35 μm; $T_0 = 80$°C. Values of $\varepsilon \equiv (d_0 - d)/d_0$ are (b) 0.037, (c) 0.213, and (d) 0.225. The horizontal dimension of the field of view in each panel is 1.1 mm.

The nature of this sequence of transverse instabilities thus clearly reveals itself in the Fourier spectra: The response of the lamellar ground state to compression and the required adjustment to the implied continuous decrease in the stripe period d involves the addition of a transverse component $q_\perp$ to the modulation wave vector $\mathbf{q} \equiv (q_\parallel, q_\perp)$, permitting its longitudinal component $q_\parallel$ to remain constant: $q_\parallel = q_\parallel(T_0) = q_0 = 2\pi/d_0$. Under continued compression, the ratio $q_\perp/q_\parallel$ approaches a limit of approximately 0.65–0.7, corresponding to typical tilt angles of 32°–35° of the "discontinuity" walls [1] in which the strain energy is localized in the fully developed chevron pattern [see Fig. 1(c)]. As in the case of smectic liquid crystals [19] these phenomena, first studied in the present context by Molho *et al.* [16], arise in magnetic-stripe patterns as a result of dilative stress, applied by tuning the modulation wave number $q = q(H,T)$ via its field or temperature dependence [16,23,24,26,27], provided the number of lamellae or stripes in the sample remains constant.

The final state of transverse distortion obtains via formation of disclination defects [26,27]. The decoration of disclinations of opposite charge in the direct space image of Fig. 1(d) reveals these to be paired into dipoles created from the discontinuity walls of the parent chevron pattern. These dipoles are aligned in a direction parallel to, and solely determined by, the wave vector $\mathbf{q} = (q_\parallel, 0)$ of the lamellar ground state. Their abrupt appearance is signaled by a pair of new, purely transverse ($q_\parallel = 0$) peaks in the diffraction pattern, which thereby acquires pseudo-sixfold symmetry [26]. As may be judged from Fig. 1(d), the dipoles are oriented so as to create pseudo-threefold symmetry about "branch" points, representing disclinations of $-\frac{1}{2}$ charge (see also Fig. 2). Both "white" and "black" components of the magnetization in the pattern contain nearly equal numbers of disclination pairs: The distribution of topological defects thus reflects, in this instance, the symmetry of the mean-field phase diagram about the axis $H = 0$ with which our experimental trajectory coincides [11,18,26]. In addition, the spatial arrangement of defects often suggests a tendency to form ordered defect arrays [19], characterized here by the appearance of rhombohedral plaquettes ("clusters") of parallel, linear segments, whose vertices are decorated by disclination dipoles [26]. The clusters' longitudinal dimension is set by the spacing of defects along the ridges of the parent chevron pattern, while the transverse dimension W reflects the transverse modulation wavelength: $W \simeq \lambda_\perp$.

A globally disordered labyrinthine state, illustrated in Fig. 2(c), evolves from the precursor pattern just described by a continuous unbinding transition of disclination dipoles, analyzed in Figs. 2 and 3. Oppositely charged disclinations, i.e., branch (△) and end (○) points exhibited by the patterns in Fig. 2, are linked by "teth-

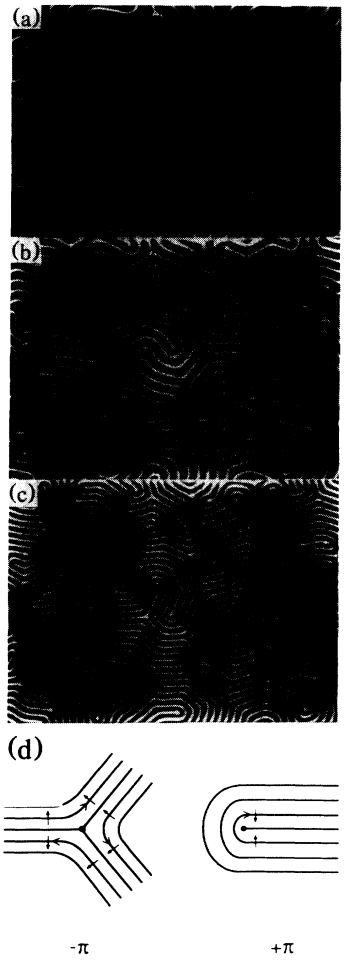

FIG. 2. Continuous "unbinding" of disclination dipoles, here driven by field-induced dilative strain at a constant temperature of 160 °C. Superimposed on the low-pass-filtered original are "tethers" linking $-\frac{1}{2}$ (Δ) and $+\frac{1}{2}$ (○) disclination charges [20]. The characteristic stripe period, $d=2\pi/q$, evaluated from azimuthally integrated 2D Fourier spectra, assumes the following values: (a) $d=25.8$ μm$\equiv d_0$, (b) $d=16.8$ μm, and (c) $d=11.5$ μm; d measures the stripe period in the direction of the local normal. The horizontal dimension of the field of view in each panel is 570 μm. (d) A sketch of the disclination defects in a layered medium [1,20]. These topological defects may be assigned a charge by noting that the layer normal (↑) undergoes a rotation through $\pm\pi=\pm\frac{1}{2}\times 2\pi$ in one circuit around a $\pm$ disclination.

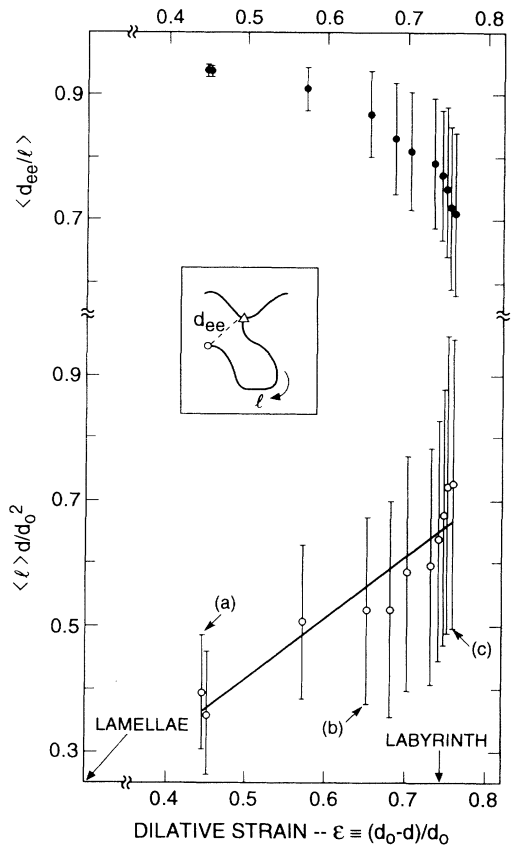

FIG. 3. Analysis of dilative-strain-mediated disclination unbinding transition. The top part of the figure illustrates the behavior of $\langle d_{ee}/l \rangle$, while the bottom part contains the evolution of the mean contour length $\langle l \rangle$ of tethers linking $+\frac{1}{2}$ and $-\frac{1}{2}$ disclination charges, shown in Fig. 2; d is computed from azimuthally averaged 2D Fourier spectra. The solid line is the result of a linear fit, discussed in the text. Vertical bars delineate $\pm\frac{1}{2}\sigma$, the pertinent mean-square deviation. The dilative strain, $\varepsilon\equiv(d_0-d)/d_0$, is defined with reference to the lamellar state (not shown) preceding Fig. 2(a); the notations (a), (b), and (c) refer to the respective panels of Fig. 2: Note that only the "white" (minority) component of each pattern was subjected to analysis.

ers" which were identified in a given image by a series of line pattern algorithms [20] and superimposed on the originals as in Figs. 2(a)–2(c): These tethers are seen to evolve from linear to curvilinear contours as their overall length increases under magnetic-field-induced compression. Under the experimental conditions pertinent here, tethers remain unbroken, and reversal of the unbinding transition recovers the original pattern.

The quantitative analysis of this disclination unbinding transition is summarized in Fig. 3 which documents the continuous evolution of, first, the mean tether contour length $\langle l \rangle$, and, second, the ratio $\langle r \rangle \equiv \langle d_{ee}/l \rangle$, a global descriptor measuring the randomization of initial dipole orientation [20,26], $0 \leq \langle r \rangle \leq 1$, and defined in terms of end-to-end distance d_{ee} and contour length; note that $r=1$ for a linear contour. Provided that the total number of disclination pairs in the sample remains constant as unbinding proceeds, simple dimensional analysis suggests that $\langle l \rangle$ scales as d^{-1}; specifically, one expects [26] $\langle l \rangle d \sim \varepsilon=(d_0-d)/d_0$, leading to the fit indicated in Fig. 3. The formation of disclination pairs at $\varepsilon\simeq 0.45$ is marked by finite jumps of both $\langle l \rangle$ (from 0) and $\langle r \rangle$ (from 1.0). As we have demonstrated elsewhere [18,20], the final, disordered pattern exhibits a well-defined structural motif, namely, an oblong polygonal plaquette or segment cluster which may be recognized as the descendant of the rhombohedral plaquette described above in connection

with Fig. 1(d).

The appearance of modulated phases in thin ferrimagnetic films may be accounted for by invoking the competition between local, attractive spin exchange and nonlocal, repulsive dipolar interactions, as demonstrated in the mean-field theory of the dipolar Ising ferromagnet given by Garel and Doniach [11]. The elastic Hamiltonian also introduced by these authors to study the formation of free dislocations in the uniaxial-stripe phase has been recently analyzed in detail by Sornette who proposes a local elastic theory of the magnetic-stripe phase derived from the "smectic" free energy [1,19,26,27], $F=F(K,B)$, given in terms of effective elastic bending (K) and compression (B) moduli. Within this framework one thus considers competing interactions to account for the selection of an optimal uniaxial modulation wave number $q_0=q_0(H,T)$ while the response of the corresponding stripe phase to subsequently imposed changes of q away from this selected value may be described, to harmonic order, by the local elastic free energy functional $F=F(K,B)$.

The findings reported here support the general validity of this concept. Remarkably, the transverse instability of the lamellar ground-state pattern in response to temperature- or magnetic-field-imposed dilative stress and the subsequent evolution of undulation and zigzag patterns, as well as the appearance of topological defects, closely follows the analogous three-dimensional scenario encountered with smectic liquid crystals [1,19]. In the present case, the two-dimensional nature of the domain patterns permits the explicit identification and tracking of topological defect positions thereby facilitating quantitative pattern analysis to follow in detail a novel strain-induced disclination unbinding transition. This is the process mediating the evolution of a labyrinthine state exhibiting global disorder while adopting a characteristic morphology and well-defined structure locally preserving the original lamellar order [18,20]. We suggest that this mechanism may be relevant to many of the uniaxially modulated systems referred to at the outset, and may perhaps play a more general role in the formation of certain glasses [28].

[1] M. Kléman, *Points, Lines and Walls* (Wiley, New York, 1983).

[2] L. A. Turkevich, in *Physics of Complex and Supramolecular Fluids*, edited by S. A. Safran and N. A. Clark (Wiley, New York, 1987), p. 241.

[3] F. S. Bates, J. H. Rosedale, and G. H. Fredrickson, J. Chem. Phys. **92**, 6255 (1990).

[4] M. E. Fisher and A. M. Szpilka, Phys. Rev. B **36**, 644 (1987).

[5] S. G. J. Mochrie, A. R. Kortan, R. J. Birgeneau, and P. M. Horn, Phys. Rev. Lett. **53**, 985 (1984); Z. Phys. B **62**, 79 (1985).

[6] E. D. Williams and N. C. Bartelt, Science **251**, 393 (1991).

[7] A. R. Sandy, S. G. J. Mochrie, D. M. Zehner, K. J. Huang, and D. Gibbs, Phys. Rev. B **43**, 4667 (1991).

[8] R. E. Rosensweig, M. Zahn, and R. J. Shumovich, J. Magn. Magn. Mater. **39**, 127 (1983).

[9] M. Seul and M. J. Sammon, Phys. Rev. Lett. **64**, 1903 (1990); M. Seul, Physica (Amsterdam) **168A**, 198 (1990).

[10] J. A. Cape and G. W. Lehman, J. Appl. Phys. **42**, 5732 (1971).

[11] T. Garel and S. Doniach, Phys. Rev. B **26**, 325 (1982).

[12] A. H. Eschenfelder, *Magnetic Bubble Technology* (Springer-Verlag, Berlin, 1986).

[13] K. L. Babcock and R. M. Westervelt, Phys. Rev. Lett. **63**, 175 (1989); **64**, 2168 (1990); Phys. Rev. A **41**, 1952 (1990).

[14] R. Seshadri and R. M. Westervelt, Phys. Rev. Lett. **66**, 2775 (1991).

[15] M. Gabay and T. Garel, J. Phys. (Paris) **46**, 5 (1985).

[16] P. Molho, J. L. Porteseil, Y. Souche, J. Gouzerh, and J. C. S. Levy, J. Appl. Phys. **61**, 4188 (1987).

[17] I. B. Puchalska, G. A. Jones, and H. Joure, J. Phys. D **11**, L175 (1978).

[18] M. Seul, L. R. Monar, L. O'Gorman, and R. Wolfe, Science **254**, 1557 (1991).

[19] N. A. Clark and R. B. Meyer, Appl. Phys. Lett. **22**, 493 (1973); R. Ribotta and G. Durand, J. Phys. (Paris) **38**, 179 (1977); Ch. S. Rosenblatt, R. Pindak, N. A. Clark, and R. B. Meyer, *ibid.* **38**, 1105 (1977); N. A. Clark and A. J. Hurd, *ibid.* **43**, 1159 (1982).

[20] M. Seul, L. R. Monar, and L. O'Gorman, Philos. Mag. A (to be published).

[21] S. Inoué, *Video Microscopy* (Plenum, New York, 1987).

[22] M. Seul, M. J. Sammon, and L. R. Monar, Rev. Sci. Instrum. **62**, 784 (1991).

[23] W. A. Barker and G. A. Gehring, J. Phys. C **16**, 6415 (1983).

[24] M. Seul and R. Wolfe (to be published).

[25] A. Weber, E. Bodenschatz, and L. Kramer, Adv. Mat. **3**, 191 (1991).

[26] M. Seul, L. R. Monar, and R. Wolfe (to be published).

[27] D. Sornette, J. Phys. (Paris) **48**, 151 (1987); **48**, 1413 (1987).

[28] P. H. Gaskell, M. C. Eckersley, A. C. Barnes, and P. Chieux, Nature (London) **350**, 675 (1991).

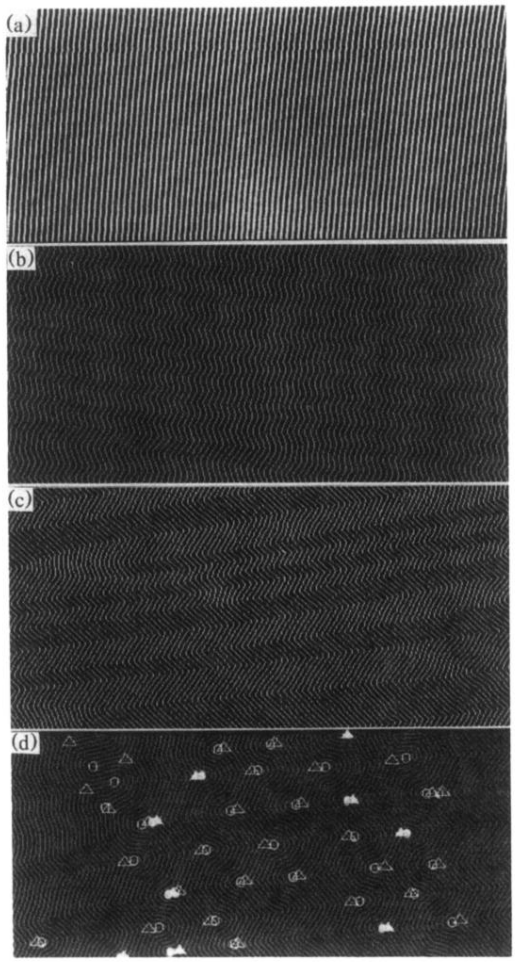

FIG. 1. (a) Transverse instability of lamellar pattern and the resulting (b) undulation and (c) chevron patterns, driven by temperature-induced dilative strain in zero field. (d) The formation of disclination dipoles in both components of the pattern ["black" (▲,●) and "white" (△,○); see also Fig. 2] generates a two-dimensional structure containing characteristic rhombohedral plaquettes. In (b)–(d), only the medial axis transform ("skeleton") [18,20] of the original "white" pattern component is shown. The stripe period, $d_0 \equiv d(T_0)$, in (a) is 35 μm; $T_0 = 80\,^{\circ}\mathrm{C}$. Values of $\varepsilon \equiv (d_0 - d)/d_0$ are (b) 0.037, (c) 0.213, and (d) 0.225. The horizontal dimension of the field of view in each panel is 1.1 mm.

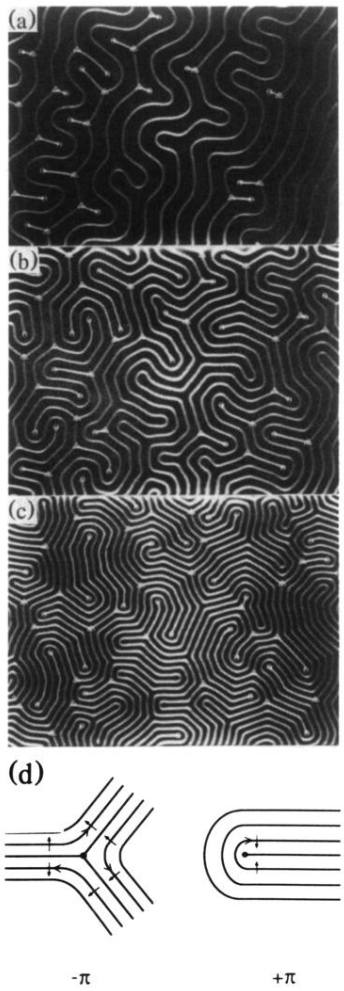

FIG. 2. Continuous "unbinding" of disclination dipoles, here driven by field-induced dilative strain at a constant temperature of 160 °C. Superimposed on the low-pass-filtered original are "tethers" linking $-\frac{1}{2}$ (Δ) and $+\frac{1}{2}$ ($\circ$) disclination charges [20]. The characteristic stripe period, $d=2\pi/q$, evaluated from azimuthally integrated 2D Fourier spectra, assumes the following values: (a) $d=25.8$ μm$\equiv d_0$, (b) $d=16.8$ μm, and (c) $d=11.5$ μm; d measures the stripe period in the direction of the local normal. The horizontal dimension of the field of view in each panel is 570 μm. (d) A sketch of the disclination defects in a layered medium [1,20]. These topological defects may be assigned a charge by noting that the layer normal ($\uparrow$) undergoes a rotation through $\pm\pi=\pm\frac{1}{2}\times 2\pi$ in one circuit around a $\pm$ disclination.